Study of Host–Guest Interactions in Intercalate Zr(HPO$_4$)$_2$ · 2CH$_3$CH$_2$OH using a Combination of Vibration Spectroscopy and Molecular Simulations

Miroslava Trchová,*,[1] Pavla Čapková,* Pavel Matějka,† Klára Melánová,‡ and Ludvík Beneš‡

*Faculty of Mathematics and Physics, Charles University, Prague, Czech Republic; † Institute of Chemical Technology, Prague, Czech Republic; and ‡Joint Laboratory of Solid State Chemistry of Academy of Sciences of the Czech Republic and University of Pardubice, Czech Republic

Vibration spectroscopy combined with molecular mechanics simulations has been used for the investigation of structural characteristics and host–guest interactions in α-zirconium phosphate intercalated with ethanol. The strategy of investigation is based on the comparison of infrared and Raman spectra for the host structure Zr(HPO$_4$) · H$_2$O, intercalated structure Zr(HPO$_4$) · 2CH$_3$CH$_2$OH, and intercalant. The analysis of infrared and Raman spectra showed that both spectra preserve the same character for the host structure Zr(HPO$_4$)$_2$ · H$_2$O and the intercalate Zr(HPO$_4$)$_2$ · 2CH$_3$CH$_2$OH. This fact led to the basic assumption of rigid layers during intercalation. The results of modeling enabled a more detailed interpretation of the vibration band profiles, revealed the character of host–guest interactions, and provided us with the structure parameters.   © **1999 Academic Press**

INTRODUCTION

α-Zirconium phosphate (for brevity α-ZrP) is a crystalline inorganic ion exchanger with many interesting physico-chemical properties (1–3). Polar organic molecules can be intercalated in the layered structure of α-ZrP and the intercalated compounds are very attractive materials, as they can be used as starting materials for pillaring, i.e., intercalating large organic molecules or inorganic complexes. These compounds may find applications in many fields, such as sorption, chemical separation and catalysis (4–6), and as new nonlinear optical materials (7). Finally the transport phenomena occurring in α-ZrP intercalates can be greatly modified by the presence of different guest molecules, and this is of interest in the field of ionic conductors and ion-exchange membranes. Intercalation of α-ZrP with ethanol leads to the formula Zr(HPO$_4$)$_2$ · 2C$_2$H$_5$OH.

The crystal packing in intercalated layered structures is ruled by the character of the interactions between the host matrix and guest molecules (2). These host–guest interactions must be stronger than the guest–guest interactions, i.e.,

the mutual interactions of the guest molecules with themselves. The surface of layers of the host structure should pose as active sites with which the guest molecules can interact. The present work focuses on the host–guest interactions and possible distortions of host layers and guest molecules as a result of intercalation. This investigation is based on the comparison of vibration spectra for the host structure and intercalate.

A study of the infrared (IR) and Raman spectra of crystalline α-zirconium phosphate has been presented by Horsley *et al.* (8). The spectra were analyzed and related to the crystal structure. The interaction between the water molecule and the lattice was discussed. Several of the bands in the IR spectra have been assigned by considering the spectral changes caused by heat treatment. In the present work the IR and Raman spectra of the host structure Zr(HPO$_4$)$_2$ · H$_2$O and its intercalate with ethanol Zr(HPO$_4$)$_2$ · 2C$_2$H$_5$OH have been measured. Combination of IR and Raman spectroscopy with the molecular mechanics simulations allows detailed analysis of the bands of vibration spectra and their interpretation.

EXPERIMENTAL

Materials

The intercalate Zr(HPO$_4$)$_2$ · 2C$_2$H$_5$OH was prepared by a reintercalation reaction from the propanol form. The replacement of water with propanol followed by reintercalation is easier than the replacement of water with ethanol. The solid propanol intercalated zirconium phosphate was prepared in advance, suspended in dry ethanol (7 ml), and exposed to the microwave field for 10 min. To obtain the pure propanol intercalated Zr(HPO$_4$)$_2$, finely ground Zr(HPO$_4$)$_2$ · H$_2$O (0.25 g) mixed with propanol (7 ml) was exposed to microwave radiation for 10 min, filtered, and mixed with a new dose of propanol, and then reexposed to microwave radiation for another 10 min. After the

preparation, intercalates were kept in closed evacuated ampoules. Their structure was checked by XRD.

Methods

Infrared measurements were carried out using a Nicolet Impact 400 Fourier transform infrared (FT-IR) spectrophotometer in a H_2O-purged environment. An ambient-temperature deuterated triglycine sulfate (DTGS) detector was used for the wavelength range 400 to 4000 cm^{-1}. A Happ–Genzel apodization function was used in all regions and the spectral resolution was 2 cm^{-1}. The baseline horizontal attenuated total reflection (HATR) accessory with ZnSe crystal was used for measurements of infrared spectra of $Zr(HPO_4)_2 \cdot H_2O$ and $Zr(HPO_4)_2 \cdot 2C_2H_5OH$. The ATR correction was made to eliminate the dependence of the effective pathlength on the wavelength.

Fourier transform Raman spectra were collected using a Fourier transform near-infrared (FT-NIR) spectrometer (Equinox 55/S, Bruker) equipped with FT Raman module (FRA 106/S, Bruker). The samples were irradiated with a focused laser beam with a laser power 100 mW of Nd-YAG (1064 nm, Coherent). The scattered light was collected in backscattering geometry. A quartz beamsplitter and Ge detector (liquid N_2 cooled) were used to obtain interferograms. One hundred twenty-eight interferograms were coadded and then processed by the Fourier transformation with Blackman–Harris four-term apodization and zerofilling factor 8 to obtain final FT Raman spectra in the range 4000 to -1000 cm^{-1} with 4 cm^{-1} resolution.

MOLECULAR MECHANICS SIMULATIONS

A Cerius^2 modeling environment was used for the molecular mechanics simulations. The initial model of the intercalate was built using the known structure of the host compound $Zr(HPO_4)_2 \cdot H_2O$ (9). After the water molecules were removed, the interlayer distance between α-ZrP layers was increased to ~ 14.5 Å in the initial model, and the ethanol molecules were placed in the bilayer arrangement into the interlayer space according to the formula $Zr(HPO_4)_2 \cdot 2C_2H_5OH$ ($Z = 4$, which means eight ethanol molecules in one unit cell). The replacement of the water molecules with ethanol in the α-ZrP interlayer during intercalation leads to the assumption that the host–guest interactions in this intercalate can be described by the nonbond terms only, which means the Crystal Packer Module in Cerius^2 modeling environment can be used. Two different calculations with different modeling strategies were carried out in the present work:

Model I: Rigid $Zr(HPO_4)_2$ layers, rigid ethanol molecules, using Crystal Packer module in Cerius^2.

Model II: Rigid $Zr(HPO_4)_2$ layers, variable bonding geometry of ethanol molecules, using Minimizer module in Cerius^2.

Model I

Crystal Packer is a computational module that estimates the total sublimation energy and packing of molecular crystals. Energy calculations in Crystal Packer take into account the nonbond terms only, i.e., van der Waals (VDW) interactions, Coulombic (COUL) interactions, hydrogen bonding (HB), internal rotations, and hydrostatic pressure. The asymmetric unit of the crystal structure is divided into fragment-based rigid units. Nonbond (VDW, COUL, HB) energies are calculated between the rigid units. During energy minimization, the rigid units can be translated and rotated and the unit cell parameters varied. In the initial model 10 rigid units have been assigned to one unit cell: two $Zr(HPO_4)_2$ layers and eight C_2H_5OH molecules.

For VDW interactions we used the well-known Lennard–Jones functional form, with the arithmetical radius combination rule. The nonbond cutoff distance for the VDW interactions was 7.0 Å. From the three force fields available in Crystal packer module—Dreiding, Universal, and Tripos—the Dreiding force field (10) has been found to be the best one for the description of VDW forces between the rigid units in our model. As the Dreiding force field available in Cerius has no VDW parameters for zirconium, we added Zr parameters for VDW term those taken from the Universal force field: 1.562 Å and 0.069 kcal/mol. [For a detailed description of the Dreiding force field see work Mayo et al. (10).]

The hydrogen bond term was a CHARM-like angle-dependent potential, with Dreiding coefficients:

$$E_{HB}(R, Q_{AHD}) = (AR^{-12} - BR^{-10}) \cos^4 Q_{AHD}. \quad [1]$$

The Ewald summation method is used to calculate the Coulombic energy in a crystal structure (11). The Ewald sum constant was 0.5 Å. Minimum charge taken into the Ewald sum was 0.00001e. All atom pairs with separation less than 10 Å were included in the real-space part of the Ewald sum and all reciprocal-lattice vectors with lengths less than 0.5 $Å^{-1}$ were included in the reciprocal part of the Ewald summation. Charges in crystal are calculated in Cerius^2 using the QEq-method (charge equilibrium approach). This method is described in detail in the original work (12). An external pressure of 99 kbar was applied for the first minimization of the initial model and then the external pressure was removed and new minimizations were started.

Model II

Burchart Universal force field was used to parametrize the model with rigid layers and variable ethanol molecules. In this case we used Model I minimized in Crystal Packer with rigid layers and rigid ethanol as an initial model and Model II for further minimization. During this minimization using the Minimizer module in Cerius^2 with variable bonding geometry of ethanol and rigid $Zr(HPO_4)_2$ layers, the cell parameters obtained from Crystal Packer were fixed.

RESULTS AND DISCUSSION

Structure of the Host Compound $Zr(HPO_4)_2 \cdot H_2O$ and Its Relation to Infrared and Raman Spectra

The structure of the host compound $Zr(HPO_4)_2 \cdot H_2O$ (α-ZrP) was determined by Clearfield and Smith (9) and refined by Troup and Clearfield (13) as monoclinic, space group $P2_1/n$, with the unit cell parameters $a = 9.060(2)$ Å, $b = 5.297(1)$ Å, $c = 15.414(3)$ Å, $\beta = 101.71(2)°$ ($Z = 4$). This compound has a layered structure in which the metal atoms lie nearly in a plane and are bridged by the phosphate groups. The unit cell contains two $Zr(HPO_4)$ layers and the interlayer distance in the host structure is 7.547 Å (see Table 1). The water molecules sit in the center of six-sided cavities in the interlayer space. Figure 1 shows the view (along the c axis) of the $Zr(HPO_4)_2$ layer with water molecules in six-sided cavities. One can see that there are two different types of these cavities, denoted I and II in Fig. 1. In type I, all the OH groups at the vertex of the PO_4 tetrahedron are oriented out of the cavity, while in type II, two OH groups are directed into the cavity. It is also evident from Fig. 1 that there are two different orientations (inclinations) of the PO_4 tetrahedron with respect to the cavities and consequently two different types of OH groups denoted A and B in Fig. 1. These nonequivalent OH groups exhibit different ways of hydrogen bonding to water molecules, as can be seen in Fig. 2. The hydration water molecules interact with three adjacent phosphate groups, accepting two hydrogen bonds and giving one. In addition, the visualization using Cerius^2 showed the existence of the fourth hydrogen bond to an oxygen atom in the Zr octahedron (see

Figs. 1 and 2). In cavity II (see Fig. 1) three hydrogen bonds of water molecule are directed to the lower layer and the fourth one is directed to the upper layer, and in cavity I the situation is reversed (three hydrogen bonds to the upper layer and one hydrogen bond to the lower layer). In such a situation a weak hydrogen bond is formed between the layers. This structural feature has its consequences in the vibration spectra, as will be explained later. The complete view of the host structure with the packing of water molecules in the interlayer space is shown in Fig. 3.

Figure 4 shows the comparison of the infrared spectra for the host compound $Zr(HPO_4)_2 \cdot H_2O$ and the intercalate $Zr(HPO_4)_2 \cdot 2C_2H_5OH$ freshly removed from the ampoule. This intercalate is unstable and, exposed to the ambient conditions, it can be easily deintercalated, which means the ethanol molecules are gradually replaced by water. Figure 4 also shows the spectra for two different stages of deintercalation exposed to ambient air for 24 h and 3 days, curves a and b. The Raman spectra are shown in Fig. 5 with three stages of deintercalation (a–c) different from stages a and b in Fig. 4. The measurements of the vibration spectra of each compound were repeated five times using five different samples of the same material. No change in the studied spectral features was observed between the results. Table 2 lists the spectra in terms of fundamental modes of the PO_4^{3-} ion and O–H stretching and bending modes (14). IR absorption between 1300 and 900 cm^{-1} of $Zr(HPO_4)_2 \cdot H_2O$ can be attributed to vibration of the orthophosphate group. The bands in the infrared spectrum at about 1070, 1045, and 1032 cm^{-1} can be assigned to the $v_1(PO_4)$ symmetric stretching vibration. These bands correspond to the two peaks at 1078 and 1053 cm^{-1} observed in the Raman spectrum (see Fig. 5). The fundamental mode $v_1(PO_4)$ in free ion (τ_d symmetry) is theoretically not degenerated and should be IR inactive. Asymmetry of the HPO_4^{2-} ion, however, makes these vibrations IR active. According to Hezel and Ross the site symmetry allows more vibration modes (15).

The $v_3(PO_4)$ antisymmetric stretching vibration appears at 1162 and 1122 cm^{-1} as very smoothed bands in the infrared spectrum. This is in good agreement with the 1138 cm^{-1} Raman frequency in the spectrum in Fig. 5. The presence of more than one band in the region of the triply

TABLE 1
Lattice Parameters of the Host Compound $Zr(HPO_4)_2 \cdot H_2O$ and the Intercalate $Zr(HPO_4)_2 \cdot 2C_2H_5OH$

Compound	Structure determined by XRD	Interlayer distance
$Zr(HPO_4)_2 \cdot 1H_2O$	Monoclinic, space group $P2_1/n$ Cell parameters: $a = 9.060$ Å, $b = 5.297$ Å, $c = 15.414$ Å, $\beta = 101.71°$	$d = 7.547$ Å
$Zr(HPO_4)_2 \cdot 2Et$	Space group $P1$ (due to the slight disorder in layer stacking) Cell parameters a and b are the same as in the host structure	$d = 14.05$ Å (obtained from XRD) $d = 14.03$ Å (obtained from modeling)
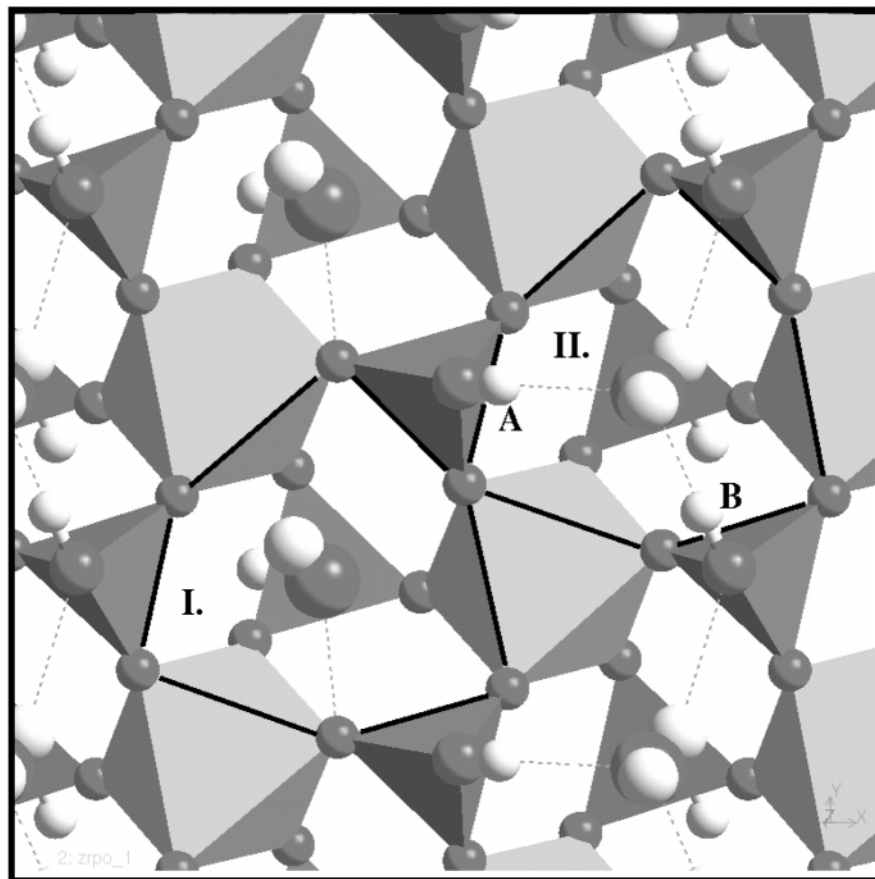
FIG. 1. View of the $Zr(HPO_4)_2$ layer in the host structure with water molecules sitting in two different six-sided cavities, denoted I and II. The two nonequivalent P–O–H groups are denoted A and B. The hydrogen bridges are marked by broken lines.

degenerate mode v_3 is probably determined by the site symmetry of the structure (15). The v_1 and v_3 frequencies of the HPO_4^{2-} ion are also influenced by the hydrogen bonding that exists between doubly charged negative phosphate ion and partially positively charged hydrogen atom of the water molecules which hydrates it (16).

The band at 1249 cm^{-1} in the infrared spectrum is due to the δ(P–O–H) in-plane deformation mode. This mode is inactive in Raman spectrum. The doublet, observed in the infrared spectrum at 962 and 957 cm^{-1} and corresponding to the δ(P–O–H) out-of-plane deformation mode, is the result of two different hydrogen bonding schemes for the OH groups A and B (see Fig. 1).

The presence of water molecules in the host compound $Zr(HPO_4)_2 \cdot H_2O$ is manifested in the infrared spectrum by the band of deformation mode at about 1615 cm^{-1} (see Table 2). In the region of stretching vibrations of the water molecule we observed broad bands at about 3310 and 3130 cm^{-1}. Two sharp peaks observed at 3500 and 3600 cm^{-1} are attributed to the (P–) O–H stretching modes corresponding to the two nonequivalent O–H groups denoted A and B in cavities I and II (see Fig. 1). The same

character of infrared spectra in this region was obtained by Mounier and Winard (17).

Structure of the Intercalate Zr(HPO₄)₂ · 2CH₃CH₂OH and Infrared and Raman Spectra

Figure 6 shows the crystal packing in the interlayer space of the intercalate obtained from the molecular mechanics simulations using Model I and Crystal Packer. The bilayer arrangement of the $Zr(HPO_4)_2 \cdot 2CH_3CH_2OH$ molecules exhibits the basal spacing $d = 14.03$ Å, which is in good agreement with the experimental value of 14.05 Å, obtained from the X-ray diffraction data (13) (see Table 1). The ethanol molecules sit in the six-sided cavities like the water molecules, bonded via hydrogen bridges to the OH groups at the vertex of the PO_4 tetrahedron. The hydrogen bonding of the ethanol molecules is different in two different cavities I and II, as can be seen in Fig. 6, where the hydrogen bonds are represented by the solid lines together with their length. As is evident from Fig. 7 each OH group is involved in two hydrogen bonds, but the bonding geometry of these bonds is different for the different OH groups, denoted A and
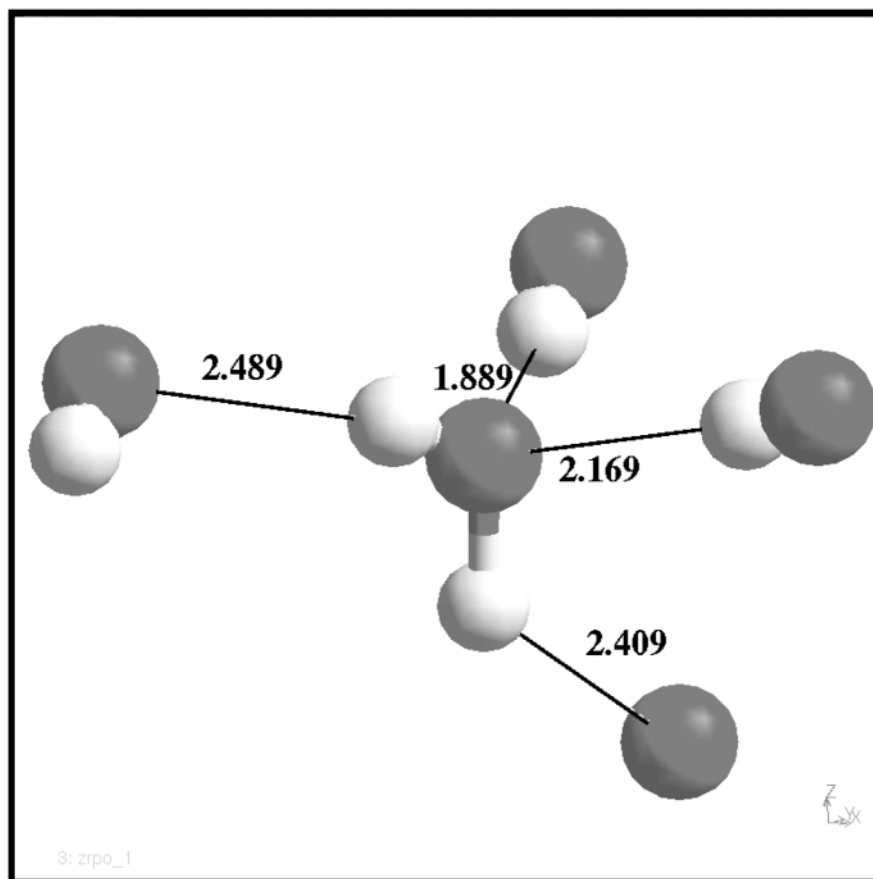
FIG. 2. View of hydrogen bonding scheme for water molecules in the host structure. Hydrogen bonds are represented by solid lines with their lengths in Å.

B in Fig. 1. The corresponding total sublimation energy per one unit cell E_{tot} represents the host–guest and guest–guest interaction energy per one unit cell. $E_{tot} = 448.7$ kcal/mol consists of the following contributions: $E_{VDW} = 39.1$ kcal/mol, $E_{COUL} = 357.8$ kcal/mol, $E_{HB} = 51.8$ kcal/mol; i.e., the electro-static contribution to the total sublimation energy is predominant. [For the complete structure analysis, including identification of disorder in layer stacking, see (18).]

Molecular simulations using Model II [rigid Zr(HPO$_4$)$_2$ layers and variable bonding geometry of ethanol] should reveal the possible effect of host–guest interactions on the intramolecular bonding of ethanol. For this purpose we compared the bonding geometry of one isolated ethanol molecule, minimized using the Burchart Universal force field, with that of an ethanol molecule minimized using the same force field in the interlayer of α-ZrP. This comparison showed that, for both ethanol molecules in cavities I and II, the distances O–H, O–C and C–C remain the same as in the case of the isolated molecule. (Changes are less than 0.01 Å·) The H–O–C angle in the isolated ethanol molecule minimized using the Burchart Universal force field was 106.3°;

for ethanol in the intercalate we found the values 106.5° in cavity I and 106.6° in cavity II.

The infrared spectra for the host compound Zr(HPO$_4$)$_2 \cdot$H$_2$O and the intercalate Zr(HPO$_4$)$_2 \cdot$2C$_2$H$_5$OH are illustrated in Fig. 4, together with the spectra of two different stages of deintercalation. These spectra together with the spectrum of pure ethanol in Fig. 4 are very helpful in the assignment of individual peaks and in their interpretation. Comparing the infrared spectra for the host structure and intercalate in Fig. 4, one can see the same character of vibration bands for both cases. The comparison of spectra exhibits many common features. The observable changes can be explained by the differences in hydrogen bonding scheme for water and ethanol molecules. Comparison of both spectra leads to the following conclusions:

● The ν_1(PO$_4$) vibration is observable in spectra of both the host structure and the intercalate in the same frequency region; however, the profile of this band is slightly modified in the infrared spectrum. This change is more pronounced in Raman spectrum (see Fig. 5). This is a consequence of the different hydrogen bonding schemes for water and ethanol molecules.
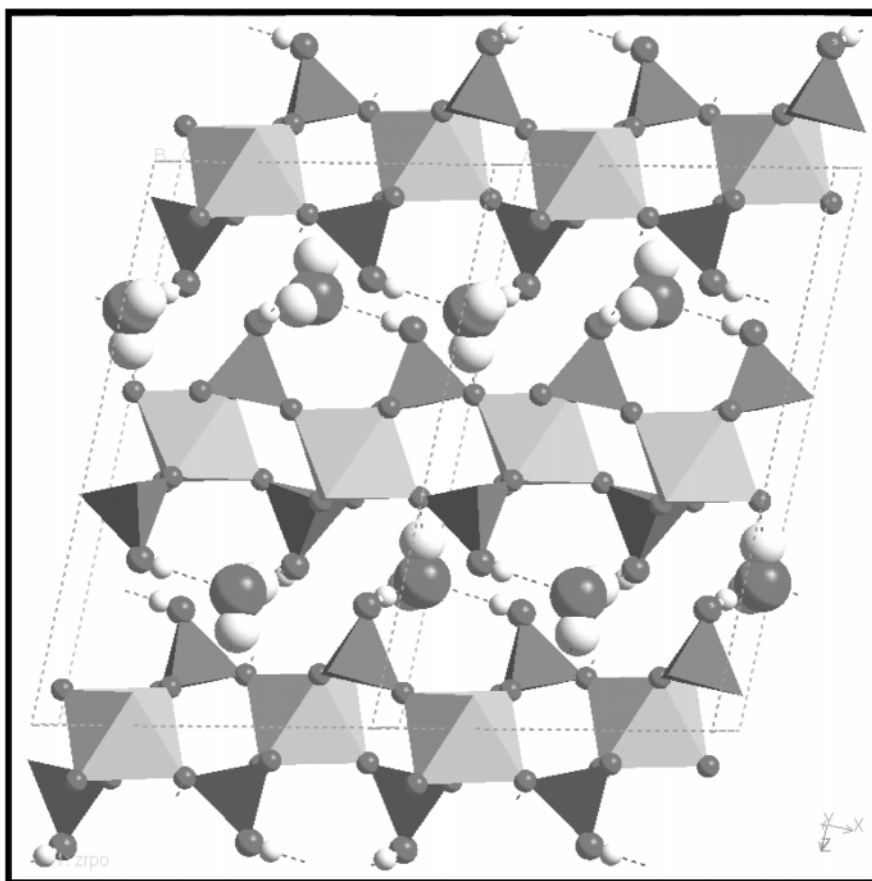
FIG. 3.   Side view of the crystal packing of the host structure $Zr(HPO_4)_2 \cdot H_2O$.

● The frequency of the the $v_3(PO_4)$ vibration mode in the Raman spectrum is only slightly shifted from 1138 to 1147 cm^{-1} going from the host structure to the intercalate.

● The band corresponding to the δ(P–O–H) in-plane deformation mode observed at 1249 cm^{-1} in the infrared spectrum of the host structure remains in the same position in the spectrum of the intercalate. This band is in the
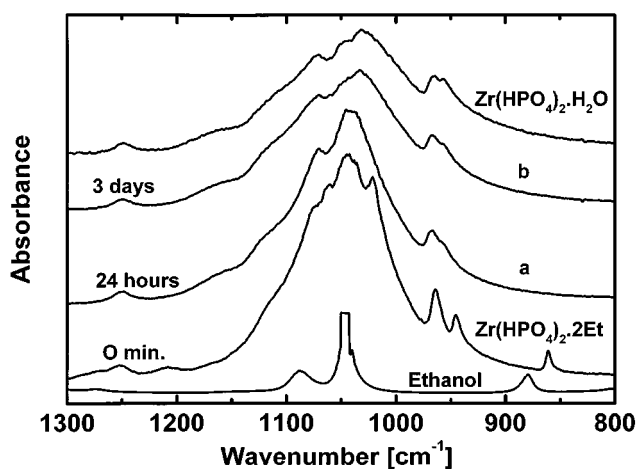

FIG. 4.   ATR infrared spectra of the host structure $Zr(HPO_4)_2 \cdot H_2O$, the intercalate $Zr(HPO_4)_2 \cdot 2C_2H_5OH$, two different degrees of deintercalation (curves a and b), and pure ethanol.
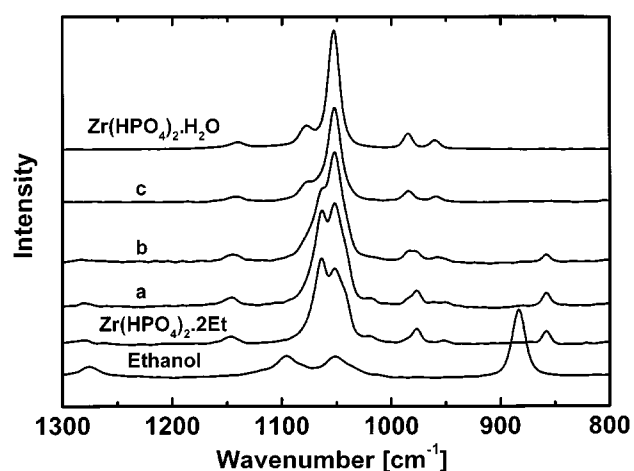

FIG. 5.   Raman spectra of $Zr(HPO_4)_2 \cdot H_2O$ and $Zr(HPO_4)_2 \cdot 2C_2H_5OH$ and its intermediate states under ambient conditions (curves a–c).

TABLE 2
Infrared (IR) and Raman (Ra) Frequencies (cm^{-1}) of $Zr(HPO_4)_2 \cdot H_2O$ and $Zr(HPO_4)_2 \cdot 2C_2H_5OH$

Vibration	$v_1(PO_4)$ symmetric stretching	$v_2(PO_4)$ symmetric bending	$v_3(PO_4)$ antisymmetric stretching	$v_4(PO_4)$ antisymmetric bending	δ_{POH} in plane	δ_{POH} out of plane	v_{HOH} v_{POH}	δ_{HOH}
$Zr(HPO_4)_2 \cdot H_2O$								
IR	1070	Not	1162	Not	1249	962	3130	1615
	1045	observable	1122	observable		957	3310	
	1032						3500 sh	
							3600 sh	
Ra	1078	293	1138	589	Inactive	985	Inactive	—
	1053			537		960		
$Zr(HPO_4)_2 \cdot 2Et$								
IR	1059	Not	1122 w	Not	1249	964	3130	—
	1045	observable	1162 vw	observable		946	3310	
	1037 w						3500 sh	
							3600 sh	
Ra	1065	293	1147	591	Inactive	978	Inactive	—
	1053			542		952		

v: very weak; w: weak; sh: sharp

infrared spectrum of the intercalate accompanied with the smoothed band at 1208 cm^{-1}. We suppose that this is the result of difference bonding of the (P)–O–H group to two different ethanol molecules in cavities I and II. This difference is more pronounced in the case of ethanol than in the case of water.
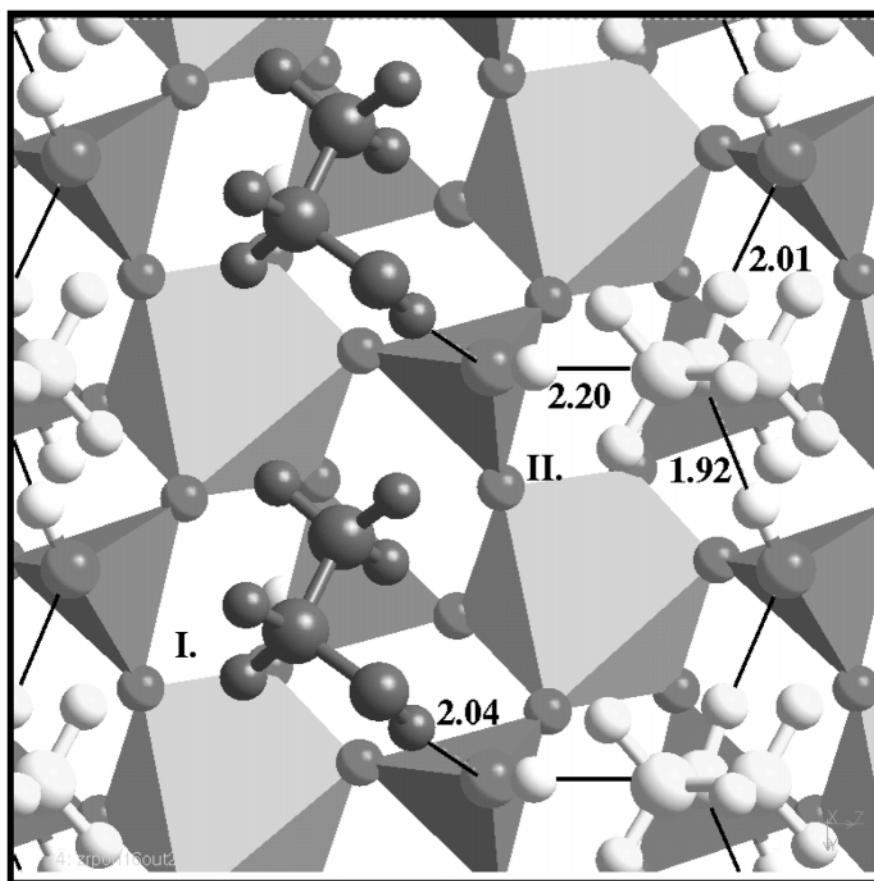
FIG. 6. View of the $Zr(HPO_4)_2$ layer in the intercalate $Zr(HPO_4)_2 \cdot 2C_2H_5OH$, with ethanol molecules positioned in two different orientations in two different six-sided cavities, denoted I and II. The hydrogen bridges are marked by solid lines with their lengths in Å.
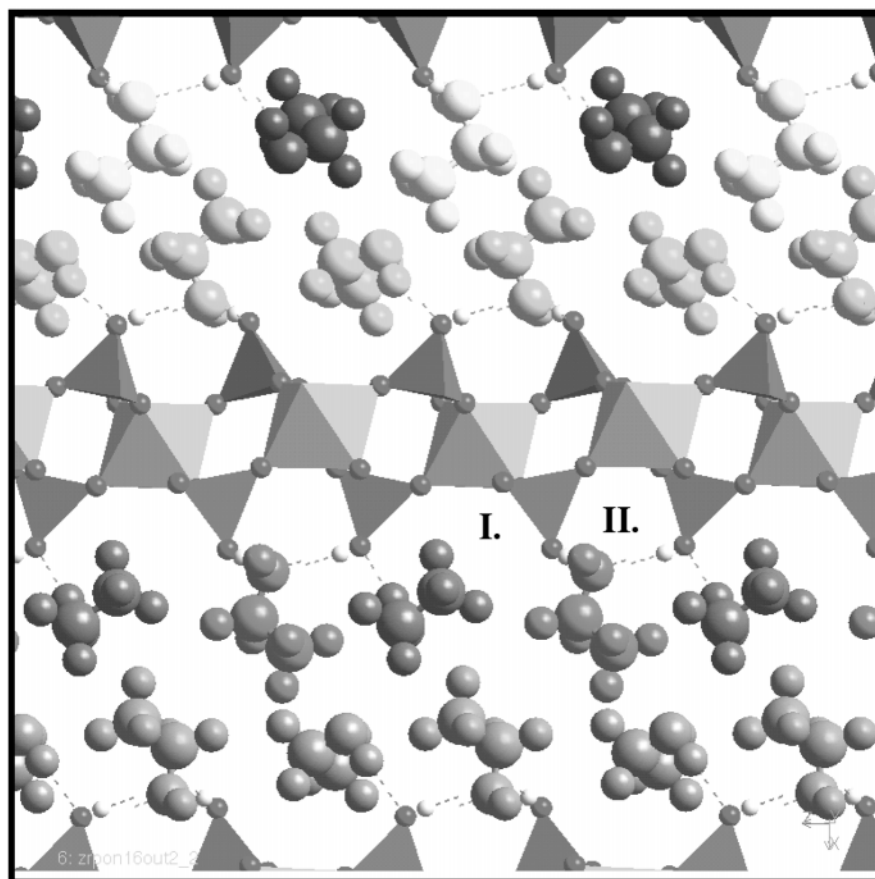
FIG. 7. Side view of the crystal packing in the intercalate $Zr(HPO_4)_2 \cdot 2C_2H_5OH$.

● The doublet $\delta(P-O-H)$ corresponding to the out-of-plane deformation mode is observable in both spectra nearly at the same position. In the case of the intercalate this doublet $\delta(P-O-H)$ is more pronounced with larger peak separation, due to the more pronounced difference in hydrogen bonding schemes between OH groups and ethanol molecules in cavities I and II. As has been mentioned by Pimentel and McClellan (19), the frequency of the out-of-plane torsion modes increased as a result of hydrogen bond formation. That means the position of the $\delta(P-O-H)$ doublet is slightly shifted to higher frequency for the host structure, as a result of stronger hydrogen bonding of water in comparison with ethanol.

● Two sharp peaks observed in the infrared spectrum of the host structure at 3500 and 3600 cm^{-1} and attributed to the (P–) O–H stretching modes remain exactly at the same position in the spectrum of the intercalate.

The infrared spectrum of the intercalate exhibits pronounced peaks corresponding to the ethanol vibrations. Frequencies of vibrations bands of pure ethanol and ethanol in the intercalate for infrared and Raman spectra are summarized in Table 3. The red shift of ethanol vibration bands

going from pure ethanol to intercalate has been observed in infrared and Raman spectra. This shift is evidently caused by the nonbonding interaction of the ethanol molecule with the $Zr(HPO_4)_2$ layer. In the host–guest interaction energy of the ethanol layer obtained from molecular simulations the electrostatic contribution prevails. The energy of hydrogen bonds is less than 10% of the total interaction energy. Nevertheless, the conclusion reached by several workers is that the C–O stretching mode of ethanol is

TABLE 3
Infrared (IR) and Raman (Ra) Frequencies (cm^{-1}) of Pure Ethanol and Ethanol in $Zr(HPO_4)_2 \cdot 2C_2H_5OH$

Ethanol	ν(C–C)	ν(C–O–H)	δ(C–O–H) in plane	δ(C–O–H) out of plane
IR				
Pure Et	1088	1049, 1040	1275	879
In $Zr(HPO_4)_2 \cdot 2Et$	1075	1019	1275	860
Ra				
Pure Et	1093	1053	1275	884
In $Zr(HPO_4)_2 \cdot 2Et$	—	1019	—	858

significantly affected by the hydrogen bond and consequently shifted to lower frequencies (19). The present molecular simulations showed that the changes in geometry of ethanol molecules in the interlayer are negligible.

CONCLUSIONS

Analysis of IR and Raman spectra showed that both spectra preserve the same character for the host structure $Zr(HPO_4)_2 \cdot H_2O$ and the intercalate $Zr(HPO_4)_2 \cdot 2CH_3CH_2OH$. This fact led to the basic assumption of rigid layers in molecular simulations. On the other hand, the results of modeling enabled the detailed interpretation of the vibration band profiles:

● The doublet $\delta(P-O-H)$ out-of-plane deformation mode in the IR and Raman spectra corresponds to two nonequivalent $(P-)O-H$ groups in $Zr(HPO_4)_2$ layers. Its profile is differently influenced by hydrogen bonding to water and ethanol molecules.

● Ethanol molecules sit in two different types of pseudohexagonal cavities with two different hydrogen bonds. This may explain the second smoothed vibration band of $\delta(P-O-H)$ out-of-plane deformation mode.

● The small shifts of $\delta(P-O-H)$ out-of-plane deformation modes observed during the replacement of ethanol molecules by water support the conclusion that the water molecules are bonded more strongly to the layers than ethanol. This results explains the low stability of the intercalate under ambient conditions.

The present study shows the necessity for combination of molecular simulations with supplementary experimental methods in the investigation of host–guest interactions.

REFERENCES

1. G. Alberti, U. Costantino, F. Marmottini, R. Vivani, P. Zappelli, *in* "Pillared Layered Structures" (I. V. Mitchell, Ed.), Elsevier Applied Science, London/New York, 1990.
2. A. Clearfield, *in* "Inorganic Ion Exchange Materials." CRC Press, Boca Raton, FL, 1982.
3. U. Costantino, *J. Chem. Soc. Dalton Trans.*, 402 (1979).
4. G. Alberti, M. Casciola, U. Costantino, R. Vivani, and P. Zappelli, *Mater. Sci. Forum* **91,** 147 (1992).
5. U. Costantino, *J. Inorg. Nucl. Chem.* **43,** 1895 (1981).
6. A. Clearfield, G. H. Nancollas, and R. H. Blessing, *in* "Ion Exchange and Solvent Extraction" (J. A. Marinsky and Y. Marcus, Eds.), Vol. 5., Chap. 1. Marcel Dekker, New York, 1973.
7. M. Ogawa, M. Takahashi, and K. Kuroda, *Chem. Mater.* **6,** 715 (1994).
8. S. E. Horsley, D. V. Nowell, and D. T. Stewart, *Spectrochim. Acta A* **30** 535 (1974).
9. A. Clearfield and D. G. Smith, *Inorg. Chem.* **8,** 431 (1969).
10. L. S. Mayo, B. D. Olafson, and W. A. Goddard III, *J. Phys. Chem.* **94,** 8897 (1990).
11. N. Karasawa and W. A. Goddard III, *J. Phys. Chem.* **93,** 7320 (1991).
12. A. K. Rappé and W. A. Goddard III, *J. Phys. Chem.* **95,** 3358 (1991).
13. J. M. Troup and A. Clearfield, *Inorg. Chem.* **16,** 3311 (1997).
14. S. D. Ross, *in* "Inorganic Infrared and Raman Spectra." McGraw–Hill, London, 1972.
15. A. Hezel and S. D. Ross, *Spectrochim. Acta* **22,** 1949 (1966).
16. S. Pinchas and D. Sadeh, *J. Inorg. Nucl. Chem.* **30,** 1785 (1968).
17. F. Mounier and L. Winard, *Bull. Soc. Chim. Fr.*, 1829 (1968).
18. P. Čapková, L. Beneš, K. Melánová, and H. Schenk, *J. Appl. Crystallogr.* (1998).
19. G. C. Pimentel and A. L. McClellan, *in* "The Hydrogen Bond." Freeman, San Francisco/London, 1960.